JOURNAL OF SPACECRAFT AND ROCKETS
Vol. 33, No. 6, November–December 1996

Space-Based Electrostatic Antenna Design with Pointing and Beam Width Control

Larry Silverberg* and Robert Stanley†
North Carolina State University, Raleigh, North Carolina 27695-7910

A new type of adaptable antenna is described that points over a 6-deg range and whose directivity is varied over a 6.5-dB range in experimental tests. The electrostatic antenna concept presented here can be regarded as a compromise between the low-performance mechanical method of adapting the far-field beam pattern and the high-performance but often prohibitively complex method of carrying out the adaptations electronically. The electrostatic antenna is shown to be well suited for space-based applications.

Nomenclature

$a_r, b_r, c_r, d_r, e_r, f_r, g_r$	= undetermined coefficients
$\boldsymbol{a}$	= vector of undetermined coefficients, $(a_0\ a_1\ a_2\ a_3\ a_4)^T$
$\boldsymbol{a}_r, \boldsymbol{x}_r$	= vectors of undetermined coefficients
f	= focal length
M	= number of test cases
r, s, i	= counting indices
T	= time constant
V	= voltage
V_1	= applied voltage pair left of center
V_2	= applied voltage pair right of center
$\boldsymbol{X}, \boldsymbol{V}$	= coefficient matrices
x	= abscissa
y	= surface deflection
$\boldsymbol{y}$	= vector of displacements
y_d	= desired surface deflection
ΔV_1	= resolution of applied voltage V_1
ΔV_2	= resolution of applied voltage V_2
Δy	= displacement error
δV	= difference between voltage pairs V_1 and V_2, $V_1 - V_2$
θ	= angle between translated and rotated axis
λ	= signal wavelength

Introduction

THE concept of deforming a thin membrane into a curved reflecting surface using electrostatic forces is old. However, until 1978 the art consisted of using a single electrode to generate the electrostatic field. On June 6, 1978, a patent was issued to Perkins.[1] The patent presented the possibility of controlling an optical surface reflector by means of multiple electrostatically charged electrodes. It also employed a supporting structure, which consisted of a large ring on which the membrane was stretched, like a circular trampoline. Perkin's supporting structure became a standard design over the next decade. The membrane tension forces had the adverse effect of requiring voltages up to 400,000 V. In addition, because of malformities in the rim, servo actuators were installed for mechanical compensation. Perkin's electrostatic antenna was later studied by Lang[2] and Goslee and Hinson[3] (see Fig. 1). The feasibility of an electrostatically controlled membrane diminished as the complexities grew and by the later 1980s all known research had ceased.

Received Aug. 1, 1995; revision received March 15, 1996; accepted for publication May 21, 1996.

*Professor, Department of Mechanical and Aerospace Engineering. Member AIAA.

†Graduate Research Assistant, Department of Mechanical and Aerospace Engineering.

The concept of harnessing electrostatic forces for membrane shaping surfaced again in the early 1990s at North Carolina State University. The first author, along with a team of graduate students, independent of the a priori work, envisioned an electrostatically shaped membrane that differed from Perkin's electrostatic membrane in one important feature. Silverberg's electrostatically shaped membrane contained no supporting structure; the outside edges were left unconstrained. This concept variation was significant enough to warrant a new patent in April 1994.[4] The research was carried out in the following progression: They were first concerned with how reliable one could predict electrostatically induced deformations.[5] The next step was a general formulation for predicting the dynamic behavior of structures subjected to electrostatic fields.[6] Once the dynamics of electrostatic structures were understood, the effort turned toward investigating control issues. One study developed a modal control technique for shaping the antenna surface to maximize the far-field power density.[7,8]

This paper focuses on the basic principles that govern the overall design of electrostatic antennas. The next section describes the performance characteristics that are achievable with the electrostatic antenna described in this paper and how these differ from a fixed shape antenna. In particular, we review the abilities of the electrostatic antenna to control pointing, directivity, and, more generally, the beam-pattern distribution. The third section provides detailed descriptions of the experimental setup, covering geometry, the membrane, power requirements, type of feed, pinned boundary conditions, back plates, measurement system, and a photo of the experiment. In the fourth section, empirical relationships that collectively govern antenna performance are developed. Surface

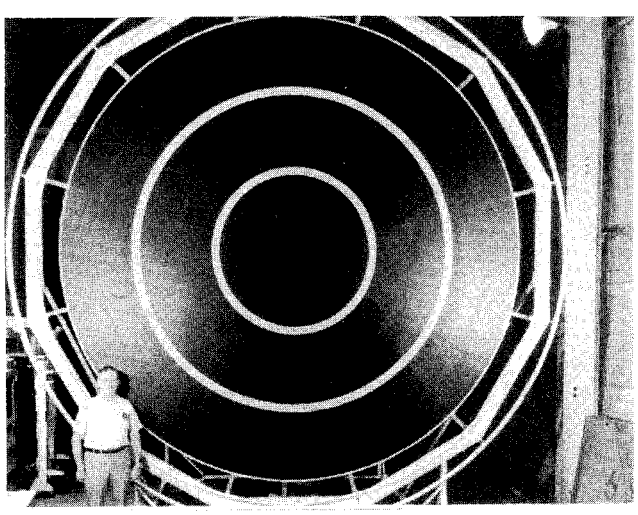

Fig. 1 Goslee's electrostatic antenna (16 ft in diameter): modified back electrode with three control areas.

deflections are expressed as a function of applied voltages, and the far-field beam pattern of the transmitted antenna signal is calculated. Voltage resolution and surface accuracy are then expressed as functions of the transmission wavelength. The fifth section gives experimental results that demonstrate the performance characteristics of the electrostatic antenna. This section shows how well the antenna beam can be pointed, its directivity varied, and its surface resolution maintained, in addition to other engineering performance characteristics.

Antenna Performance

The earliest human-made far-field antennas date back to the 1920s with the ability to transmit and receive short wavelength signals for radio detection. Monopole and dipole antennas were first used and later directional antennas were designed to yield desirable beam patterns. Then next level of sophistication in antenna design arose with the introduction of adaptable antennas wherein the beam pattern is adapted in real time. Adaptable antennas are currently one of two types: mechanical or electronic (phased array). This paper describes another type of adaptable antenna, called an electrostatic antenna, that is particularly well suited for space-based applications.

Unlike the mechanical and electronic types, the electrostatic antenna's beam pattern is adapted by varying the shape of the antenna's surface, specifically, its modes of deformation. The first mode of deformation is called the pointing mode. This mode is responsible for global beam pointing. The pointing mode enables the antenna to scan and to function for surveillance and mapping purposes. The second mode of deformation controls the beam width. In space applications, the beam width mode controls the ground swath illuminated on the Earth by the antenna. The beam width mode is useful in communication satellites and in certain military applications. Higher modes of deformation control the general power distribution of the beam.

Within the context of space-based adaptable antennas, the mechanical types tend to suffer from the following limitations. Their beam pattern adaptability is restricted to pointing (mode one deformation), and the associated beam pattern time constants are relatively large ($T > 500$ s). On the other hand, the electronic types can control the beam pattern rapidly ($T < 1$ ms), but heat rejection problems and other manufacturing complexities have inhibited their use. The electrostatic antenna, as this paper demonstrates, is capable of controlling the first two modes of the beam pattern (pointing and beam width). The control of the higher modes has not yet been demonstrated, although it is feasible, in principle. The associated time constants are smaller than for the mechanical type and larger than for the electronic type. The relatively small beam pattern time constants associated with electrostatic antenna ($T < 10$ s) are achievable because the aperture is composed of a low-mass membrane that is weakly coupled to the satellite dynamics.

Setup

An electrostatic antenna works on the basic principle that like charges repel. When two electrodes are charged, with one fixed and one free to move, the free electrode will move apart from the fixed electrode so as to balance the elastic restoring force and the electrostatic force. By controlling the applied voltages, the position of the free electrode can be prescribed. On this basis, an electrostatic antenna is designed here to control its first two modes of deformation, which in turn control pointing and beam width (Fig. 2).

In the following experiment, the fixed electrodes (see 2 and 4 in Fig. 3) are referred to as back plates, and the free electrodes (see 3 and 5 in Fig. 3) are electrically segmented regions on a 7-mil metalized Mylar® membrane. Metalized Mylar was chosen because it is elastic, conductive, and easily segmented. Metal between segments was removed using a liquid solution of sodium bydroxide (NaOH) (Fig. 4).

The membrane is physically constrained by a magnetically levitated pinned support (see 6 in Fig. 3). The support is composed of two semicylinders that form a cylinder when brought together (1-in. diam, 13-in. length). Seven pairs of attracting magnets secure the centerline of the membrane along the constrained interproximal surface via $\frac{1}{4}$-in. holes bored into the support as seen in Fig. 2 (see also Fig. 5). Along the long axis of the cylinder there exist alternating regions of insulative and conductive material (see 7 and 8 in Fig. 5, respectively). These regions provide a conductive pathway along which the membrane segments are charged. The support is constrained in the horizontal plane by high-precision ball bearings (see 9 in Fig. 5). In the vertical direction the support is levitated by neodymium-iron-boron magnets. This combination produces a near frictionless pinned boundary condition at the center of the membrane while allowing the edges to freely deflect.

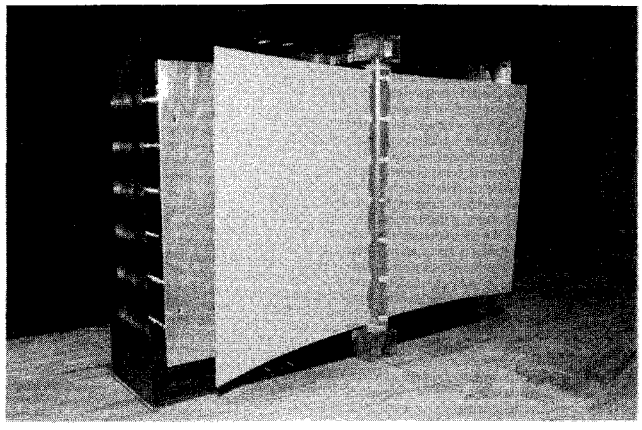

Fig. 2 Electrostatic antenna (18 in. wide, 12 in. high, and 4 in. deep).

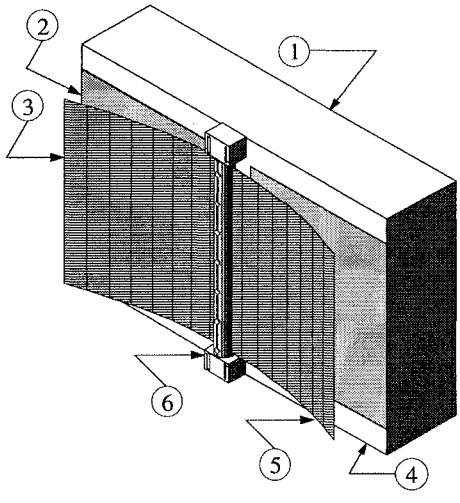

Fig. 3 Test block and membrane apparatus: 1) high-voltage test block, 2) left-hand side back plate, 3) left-hand side of electrically segmented metalized Mylar, 4) right-hand side back plate, 5) right-hand side of electrically segmented metalized Mylar, and 6) magnetically levitated pinned boundary conditions.

The back plates are composed of thin aluminum rectangular plates; however, just about any conductive material would work. The number of back plates is governed by the number of controlled modes of deformation, in this experiment two. As a general rule, the number of independently controlled back plates is not less than the number of controlled modes of deformation. In optical applications, the surface tolerance requirements may not be met with the minimum number of back plates, in which case more back plates are used until the desired surface accuracy is reached. In microwave applications, the number of controlled back plates is on the order of the number of controlled modes of deformation. Since we seek to control two modes, we use two back plates, each paired with one side of the membrane. Also note that the fixed back plates may be eliminated in some designs by instead using attached back plates.[4]

The back plates along with the support are mounted on a multipurpose high-voltage test block. The test block consists of nothing more than an $18 \times 12 \times 4$ in. block of acrylic with uniformly spaced holes that accept spring loaded RJ-8 coaxial cables from 0–30 kV dc power supplies. The springs act as motor brushes, which allow the two parts of the membrane to be charged while not inhibiting the motion.

Antenna surface test measurements were gathered with a linear positioning device and an analog optical distance sensor with a

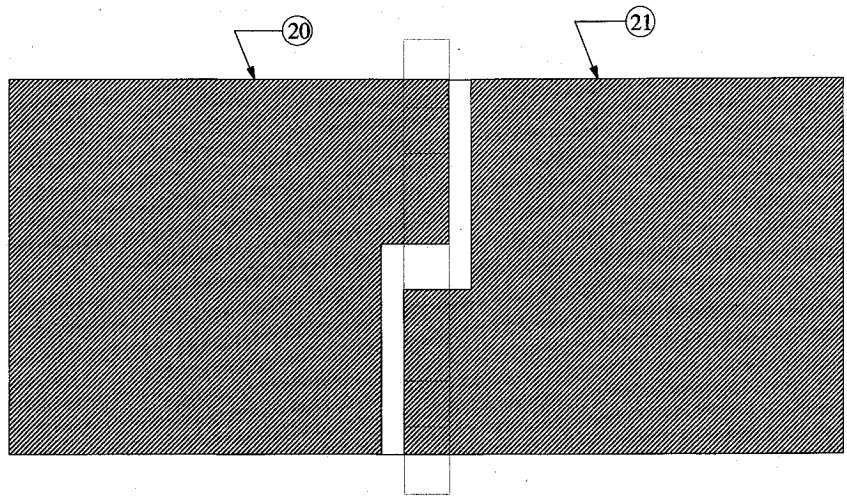

Fig. 4 Electrically segmented metalized Mylar: 20) left-hand side of electrically segmented metalized Mylar and 21) right-hand side of electrically segmented metalized Mylar.

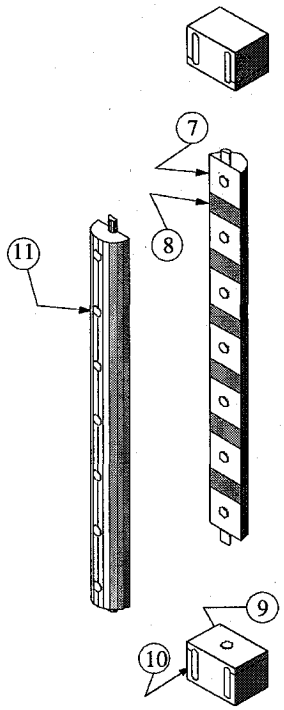

Fig. 5 Magnetically levitated pinned support: 7) insulative material, 8) conductive material, 9) high-precision ball bearing and magnet well, 10) high-voltage test block mounting slots, and 11) attracting magnets.

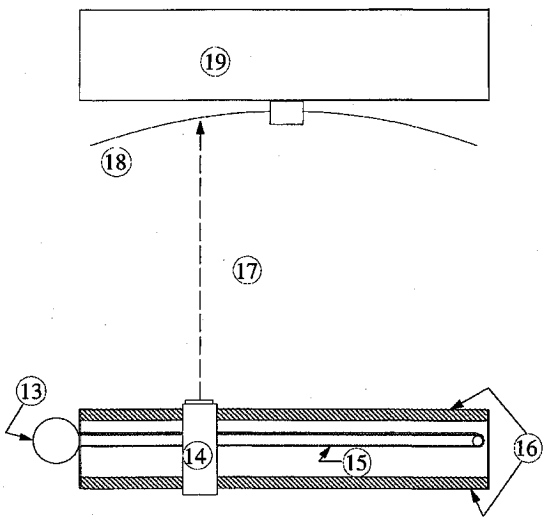

Fig. 6 Test setup overview: 13) stepper motor, 14) SA1D analog optical distance sensor, 15) drive belt, 16) slider rods, 17) SA1D sensor line of sight, 18) metalized Mylar membrane, and 19) high-voltage test block.

Table 1 Applied voltages for each scan ($M = 11$)

	V_2, kV				
V_1, kV	0	5	10	15	20
0	X				
5		X			
10		X	X		
15		X	X	X	
20		X	X	X	X

resolution of 0.034 in. The analog distance sensor rides broadside to the aperture on the linear positioner via a carriage. By recording the 0–5 V analog output signal from the sensor at specified intervals, the antenna surface is recorded (Fig. 6).

Engineering Curves

The engineering performance of the electrostatic antenna is described by relationships (curves) between the applied voltages, the surface deformations, and the beam pattern. First, the surface deformations are expressed as a function of the applied voltages. Next, beam pattern parameters are expressed as functions of the surface deformations. Finally, surface rms values and resolution issues are discussed.

The deformation of a surface cross section is assumed in the polynomial form

$$y(x, V_1, V_2) = \sum_{r=0}^{4} a_r(V_1, V_2)x^r, \qquad x_1 \le x \le x_N \quad (1)$$

where

$$a_r(V_1, V_2) = b_r + V_1 c_r + V_2 d_r + V_1^2 e_r + V_2^2 f_r + V_1 V_2 g_r \quad (2)$$

The previously described measurement system scans the membrane and records surface deformations at x_s ($s = 1, 2, \ldots, N$). The measurement system scans the membrane $M = 11$ distinct times; each time the applied voltages V_1 and V_2 are updated (Table 1). Deformation curves are obtained from the data in two steps. The first step determines a_r ($r = 0, 1, \ldots, 4$) in Eq. (1) for each scan. The second step determines b_r, c_r, d_r, f_r, and g_r ($r = 0, 1, \ldots, 4$) as a function of V_1 and V_2. For each scan, the first step yields from Eq. (1) the set of linear algebraic equations

$$\boldsymbol{Xa} = \boldsymbol{y} \quad (3)$$

in which $\boldsymbol{a} = [a_0 \ a_1 \ \cdots \ a_4]^T$, $\boldsymbol{y} = [y(x_1) \ y(x_2) \ \cdots \ y(x_N)]^T$, and

$$\boldsymbol{X} = \begin{bmatrix} 1 & x_1 & x_1^2 & x_1^3 & x_1^4 \\ 1 & x_2 & x_2^2 & x_2^3 & x_2^4 \\ \vdots & \vdots & \vdots & \vdots & \vdots \\ 1 & x_N & x_N^2 & x_N^3 & x_N^4 \end{bmatrix}$$

Table 2 Deflection coefficients vs r ($r = 0, 1, 2, 3, 4$)

	0	1	2	3	4
b_r	1.3449e+01	3.0670e−01	−4.7906e−02	3.8650e−03	−1.4097e−04
c_r	−1.3185e−02	4.1077e−03	−7.8032e−05	−5.6697e−05	3.2718e−06
d_r	−1.9472e−03	7.6749e−04	−5.4300e−04	9.4436e−05	−4.6386e−06
e_r	−8.7081e−04	2.1771e−04	−3.0525e−05	3.3055e−06	−1.3254e−07
f_r	1.6006e−03	−2.6937e−04	−5.5771e−06	2.9624e−06	−1.6797e−07
g_r	−1.3268e−03	6.9404e−05	7.9863e−05	−1.2268e−05	5.0688e−07

The least squares estimate of $\boldsymbol{a}$ is given by

$$\boldsymbol{a} = (\boldsymbol{X}^T\boldsymbol{X})^{-1}\boldsymbol{X}^T\boldsymbol{y} \tag{4}$$

The second step yields from Eqs. (2) and (4) the set of linear algebraic equations

$$\boldsymbol{V}\boldsymbol{z}_r = \boldsymbol{a}_r, \qquad (r = 0, 1, \ldots, 4) \tag{5}$$

in which $\boldsymbol{a}_r = [a_r(1) \quad a_r(2) \quad \cdots \quad a_r(M)]^T$, $z_r = [b_r, c_r, d_r, e_r, f_r, g_r]^T$, and

$$\boldsymbol{V} = \begin{bmatrix} 1 & V_1(1) & V_2(2) & V_1^2(1) & V_2^2(1) & V_1(1)V_2(1) \\ 1 & V_1(2) & V_2(2) & V_1^2(2) & V_2^2(2) & V_1(2)V_2(2) \\ 1 & V_1(3) & V_2(3) & V_1^2(3) & V_2^2(3) & V_1(3)V_2(3) \\ \vdots & \vdots & \vdots & \vdots & \vdots & \vdots \\ 1 & V_1(M) & V_2(M) & V_1^2(M) & V_2^2(M) & V_1(M)V_2(M) \end{bmatrix}$$

Finally, the least squares estimates of z_r ($r = 0, 1, \ldots, 4$) are given by

$$z_r = (\boldsymbol{V}^T\boldsymbol{V})^{-1}\boldsymbol{V}^T\boldsymbol{a}_r, \qquad (r = 0, 1, \ldots, 4) \tag{6}$$

The surface deformations described earlier were obtained empirically rather than predicted from a physical model of the system. The prediction of surface deformations of electrostatic structures is possible but was unnecessary in this investigation.[6]

Having expressed deformations as functions of the applied voltages, the next step is to determine the far-field beam pattern and its associated performance parameters (pointing, beam width, etc.) as a function of the surface deformations. Rather than perform this part of the investigation experimentally, we turned to a very accurate method of prediction that is based on physical optics. Many commercially available computer subroutines exist; in our study we used POMESH.[9]

Another useful set of parameter curves governs surface deformation sensitivity. The rms value of the difference between the actual surface deformation and the desired surface deformation is determined in several steps. The surface deformations are first translated to a set of axes whose origin lies on the vertex of the membrane. A weighted average of the pointing of the surface deformations are then determined by

$$\theta = \frac{1}{2}\frac{\sum_{i=1}^{N/2}[y(x_i) - y(-x_i)]x_i}{\sum_{i=1}^{N/2}x_i^2} = \frac{\sum_{i=1}^{N/2}\theta_i x_i^2}{\sum_{i=1}^{N/2}x_i^2} \tag{7}$$

in which $\theta_i = [y(x_i) - y(-x_i)]/2x_i$ denotes the pointing angle associated with x_i and $-x_i (x_i > 0)$. Note that θ also represents the least squares solution obtained by minimizing the error functional

$$E = \sum_{i=1}^{N/2}[y(x_i) - y(-x_i) - 2\theta x_i]^2$$

$$= \sum_{i=1}^{N/2}\{[y(x_i) - \theta x_i] - [y(-x_i) + \theta x_i]\}^2$$

The translated coordinates are now rotated an amount θ. The desired surface deformations in the rotated frame are given by the general parabolic form $y_d = (1/4f)x^2$, and the associated rms value of the difference between the actual surface deformation and the desired surface deformation is given by

$$\text{rms}_1 = \left\{\frac{1}{N}\sum_{r=1}^{N}[y(x_r, V_1, V_2) - y_d(x_r, V_1, V_2)]^2\right\}^{\frac{1}{2}} \tag{8}$$

in which $y_d(x_r, V_1, V_2)$ denotes the desired surface deformation as a function of x_r, V_1, and V_2 in the rotated coordinate system. Another rms value of importance is associated with the error introduced by the limiting resolution of the applied voltages V_1 and V_2. We obtain

$$\text{rms}_2 = \left\{\frac{1}{N}\sum_{r=1}^{N}\left[\frac{\partial y(x_r, V_1, V_2)}{\partial V_1}\Delta V_1 + \frac{\partial y(x_r, V_1, V_2)}{\partial V_2}\Delta V_2\right]^2\right\}^{\frac{1}{2}} \tag{9}$$

in which the inner parenthetic term denotes the displacement error $\Delta y(x_r, V_1, V_2)$. Both rms errors given in Eqs. (8) and (9) contribute independently to the total rms error

$$\text{rms} = \text{rms}_1 + \text{rms}_2 \tag{10}$$

The transmitted or received signal that coherently reflects off of the aperture bounds the total rms by

$$\text{rms} < \lambda/10 \tag{11}$$

Equation (1) determines the surface deformations as functions of the applied voltages, which in turn are related to the beam pattern, as previously described, and the surface deformations are related to acceptable rms levels as indicated by Eq. (11).

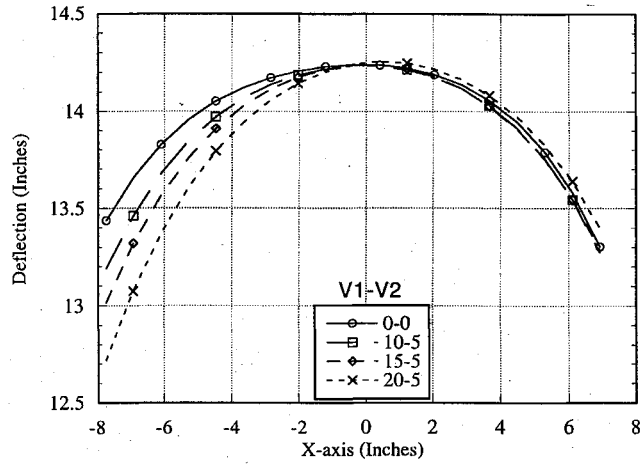

Fig. 7 Pointing mode.

Performance Tests

The electrostatic antenna described in this paper was designed to undergo the first two modes of deformation: the pointing mode and the beam width mode. Upon completing $M = 11$ independent scans, the antenna's deformation as a function of position and applied voltage pairs V_1 and V_2 [Eqs. (1) and (2)] were computed. The results are given in Table 2, in which the origin was shifted 8 in. to the right. The simulated far-field patterns used a transmission frequency of 1 GHz ($\lambda = 18.80$ in.) and a dipole feed. We first evaluate the pointing mode. As shown in Fig. 7 and referring to Table 1, the rotation of the antenna is proportional to the difference between the applied

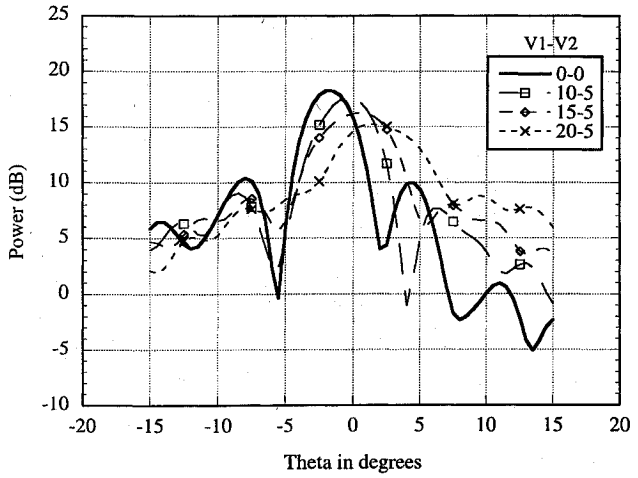

Fig. 8 Beam pattern (pointing mode).

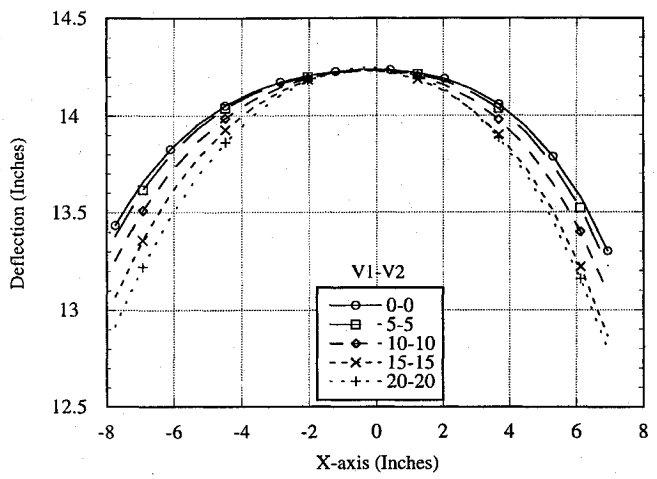

Fig. 9 Beam width mode.

voltage to the left of center (V_1) and the applied voltage to the right of center (V_2), denoted by $\delta V = V_1 - V_2$. From Fig. 7 the antenna rotates approximately 1 deg every $\delta V = 5$ kV. The associated beam pattern is shown in Fig. 8. As shown, the pointing also increases approximately 1 deg every $\delta V = 5$ kV. This corresponds to the best parabolic fit to the uncharged preshaped membrane ($V_1 = V_2 = 0$). The desired antenna surface was assumed to be parabolic with a focal length of $f_0 = 15.84$ in. The rms values corresponding to Fig. 7 are $\text{rms}_1 = (0.47, 0.54, 0.58, 0.62)$.

The rms values for the other test cases were similar. The rms values associated with the voltage resolution determined from Eq. (8) were small compared with the rms values associated with the parabolic fit. The implication is that the performance of the power source met the antenna requirements. From Eq. (10), the useful transmitting or receiving wavelengths are bounded by $\lambda_{\min} = 6.2$ in.

The evaluation of the beam width mode is now described. As shown in Fig. 9, and referring to Table 1, the focal length is inversely proportional to the uniformly applied voltage $V = V_1 = V_2$. From Fig. 10, the associated power density decreased by approximately 6.5 dB as the applied voltage increased by 20 kV. As before, the desired surface was assumed to be the best parabolic function that fit the uncharged surface of the membrane. The associated rms values were $\text{rms}_1 = (0.47, 0.51, 0.54, 0.70, 0.76)$. Once again $\text{rms}_2 \ll \text{rms}_1$,

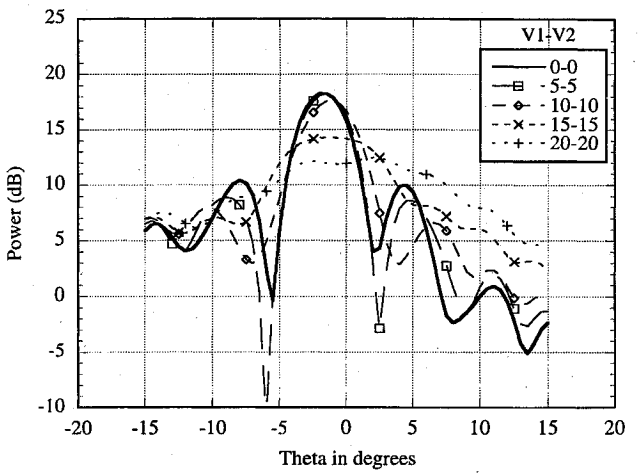

Fig. 10 Beam pattern (beam width mode).

and the beam width mode met the antenna wavelength requirements bounded below by $\lambda_{\min} = 7.6$ in.

Summary

This paper described the design of an experimental electrostatic antenna and tested its performance. The experimental antenna was shown to be capable of adapting the pointing of the main beam over a 6-deg range and the beam width over a 6.5-dB range. The experimental antenna surface was sufficiently accurate to accommodate wavelengths bounded below by approximately 7.6 in.

Future efforts could extend the results presented here to the design and testing of electrostatic antennas that are paraboloidally preshaped and to the increase of the number of independently applied voltages along with an increase in the number of modes of deformation that are shaped.

Acknowledgment

This research is supported by NASA Grant NAGW-1331 to the Mars Mission Research Center.

References

[1]Perkins, C. W., "Controlled Flexible Membrane Reflector," U.S. Patent 4,093,351, June 1978.

[2]Lang, J. H., Staelin, D. H., and Johnson, T. L., "The Experimental Computer Control of a Two-Dimensional Hyperbolic System," *IEEE Transactions on Automatic Control*, Vol. 33, No. 1, 1988, pp. 79–87.

[3]Goslee, J. W., Hinson, W. E., and Davis, W. T., "Electrostatic Forming and Testing of Polymer Films on a 16-Foot Diameter Test Fixture," NASA TM 86328, Feb. 1985.

[4]Silverberg, L., "Electrostatically Shaped Membranes," U.S. Patent 5,307,082, April 1994.

[5]Silverberg, L., and Doggett, W. O., "Planar Electrodynamics of Interconnected Charged Particles," *American Physical Society Bulletin*, Series 2, Vol. 36, No. 10, 1991, p. 2737.

[6]Silverberg, L., and Weaver, L., "Dynamics and Control of Electrostatic Structures," *Journal of Applied Mechanics*, Vol. 63, June 1996, pp. 383–391.

[7]Silverberg, L., and Washington, G., "Modal Control of Reflector Surfaces Using Far-Field Power Measurements," *Microwave and Optical Technology Letters*, Vol. 7, No. 12, 1994, pp. 588–593.

[8]Washington, G., and Silverberg, L., "Modal Control of a Corner Reflector to Maximize Far-Field Power," *Microwave and Optical Technology Letters*, Vol. 8, No. 5, 1995, pp. 260–264.

[9]Anon., "POMESH," Computer Software Management and Information Center, Univ. of Georgia, Athens, GA, 1985.

H. R. Anderson
Associate Editor